



ACCEPTED MANUSCRIPT

# A versatile embedding medium for freeform bioprinting with multi-crosslinking methods

To cite this article before publication: Qi Li *et al* 2022 *Biofabrication* in press <https://doi.org/10.1088/1758-5090/ac7909>

## Manuscript version: Accepted Manuscript

Accepted Manuscript is "the version of the article accepted for publication including all changes made as a result of the peer review process, and which may also include the addition to the article by IOP Publishing of a header, an article ID, a cover sheet and/or an 'Accepted Manuscript' watermark, but excluding any other editing, typesetting or other changes made by IOP Publishing and/or its licensors"

This Accepted Manuscript is © 2022 IOP Publishing Ltd.

During the embargo period (the 12 month period from the publication of the Version of Record of this article), the Accepted Manuscript is fully protected by copyright and cannot be reused or reposted elsewhere.

As the Version of Record of this article is going to be / has been published on a subscription basis, this Accepted Manuscript is available for reuse under a CC BY-NC-ND 3.0 licence after the 12 month embargo period.

After the embargo period, everyone is permitted to use copy and redistribute this article for non-commercial purposes only, provided that they adhere to all the terms of the licence <https://creativecommons.org/licenses/by-nc-nd/3.0>

Although reasonable endeavours have been taken to obtain all necessary permissions from third parties to include their copyrighted content within this article, their full citation and copyright line may not be present in this Accepted Manuscript version. Before using any content from this article, please refer to the Version of Record on IOPscience once published for full citation and copyright details, as permissions will likely be required. All third party content is fully copyright protected, unless specifically stated otherwise in the figure caption in the Version of Record.

View the [article online](#) for updates and enhancements.

# A Versatile Embedding Medium for Freeform Bioprinting with Multi-Crosslinking Methods

Qi Li<sup>1,2,5</sup>, Zhuoran jiang<sup>3,5</sup>, Liang Ma<sup>1,2,5</sup>, Jun Yin<sup>1,2</sup>, Ziqi Gao<sup>1,2</sup>, Luqi Shen<sup>4</sup>, Huayong Yang<sup>1,2</sup>, Zhanfeng Cui<sup>3</sup>, Hua Ye<sup>3,6</sup> and Hongzhao Zhou<sup>1,2,6</sup>

<sup>1</sup> State Key Laboratory of Fluid Power and Mechatronic Systems, Zhejiang University, Hangzhou, 310058, People's Republic of China

<sup>2</sup> School of Mechanical Engineering, Zhejiang University, Hangzhou, 310058, People's Republic of China

<sup>3</sup> Institute of Biomedical Engineering, Department of Engineering Science, University of Oxford, OX3 7DQ, UK

<sup>4</sup> Key Laboratory of Growth Regulation and Translational Research of Zhejiang Province, School of Life Sciences, Westlake University, Hangzhou, 310024, People's Republic of China

<sup>5</sup> These authors contributed equally as first authors.

<sup>6</sup> Authors to whom any correspondence should be addressed.

E-mail: [hz\\_zhou@zju.edu.cn](mailto:hz_zhou@zju.edu.cn), [hua.ye@eng.ox.ac.uk](mailto:hua.ye@eng.ox.ac.uk)

Received xxxxxx

Accepted for publication xxxxxx

Published xxxxxx

## Abstract

Embedded freeform writing addresses the contradiction between the material printability and biocompatibility for conventional extrusion-based bioprinting. However, the existing embedding mediums have limitations concerning the restricted printing temperature window, compatibility with bioinks or crosslinkers, and difficulties on medium removal. This work demonstrates a new embedding medium to meet the above demands, which composes of hydrophobically modified hydroxypropylmethyl cellulose (H-HPMC) and Pluronic F-127 (PF-127). The adjustable hydrophobic and hydrophilic associations between the components permit tunable thermoresponsive rheological properties, providing a programable printing window. These associations are hardly compromised by additives without strong hydrophilic groups, which means it is compatible with the majority of bioink choices. We use polyethylene glycol 400, a strong hydrophilic polymer, to facilitate easy medium removal. The proposed medium enables freeform writing of the millimetric complex tubular structures with great shape fidelity and cell viability. Moreover, five bioinks with up to five different crosslinking methods are patterned into arbitrary geometries in one single medium, demonstrating its potential in heterogeneous tissue regeneration. Utilizing the rheological properties of the medium, an enhanced adhesion

1  
2  
3 writing method is developed to optimize the structure's strand-to-strand adhesion. In  
4 summary, this versatile embedding medium provides excellent compatibility with  
5 multi-crosslinking methods and a tunable printing window, opening new opportunities  
6 for heterogeneous tissue regeneration.  
7  
8  
9

10 **Keywords:** 3D bioprinting, embedding medium, freeform writing, tissue regeneration  
11  
12  
13  
14  
15  
16  
17  
18  
19  
20  
21  
22  
23  
24  
25  
26  
27  
28  
29  
30  
31  
32  
33  
34  
35  
36  
37  
38  
39  
40  
41  
42  
43  
44  
45  
46  
47  
48  
49  
50  
51  
52  
53  
54  
55  
56  
57  
58  
59  
60

1  
2  
3  
4 **1. Introduction**

5  
6 The three-dimensional (3D) bioprinting has been considered as a revolutionizing  
7 manufacturing strategy for regenerative medicine due to its capabilities to combine  
8 cells, biomaterials, bioactive molecules precisely, and to pattern them into 3D structures  
9 arbitrarily [1-3]. Among the major bioprinting technologies, extrusion-based  
10 bioprinting is most commonly used, which could deposit a wide range of materials and  
11 allow low-cost and high-precision fabrication of cell-laden scaffolds with high cell  
12 viability [4, 5]. However, controversy exists regarding the material printability and cell  
13 functionality in a conventional extrusion-based bioprinting process. High material  
14 stiffness is required to maintain the prescribed 3D shape integrity and fidelity under  
15 gravity, whereas it will usually come with reduced cell capabilities, including cell  
16 adhesion, migration, and proliferation [1]. Soft materials with great biocompatibility  
17 usually lack printability. It is therefore difficult to fabricate complex structures in the  
18 air with these kinds of materials. Changing the supporting medium from air to  
19 embedding medium to keep the extruded bioink in situ prior to gelation is an emerging  
20 strategy, which refers to as freeform writing or embedded printing [6]. The medium  
21 exhibits solid-like properties below its yield stress, while it fluidizes upon the shear  
22 stress exceeding its yield stress, which allows the deposition of the bioink. Following  
23 the removal of the applied stress, the medium recovers to its solid-like status quickly to  
24 keep the deposited bioink in situ before crosslinking. Considering its advantages, such  
25 an embedded printing approach has already been applied to fabricate hollow structures  
26 [7], 3D structures with overhangs or internal voids [8-10], and even complex human  
27 organs or tissue models [11-14].

28  
29 Although previously reported embedding mediums are suitable for some specific  
30 applications, they all have their own limitations. The embedding mediums can be  
31 classified into bulk gel medium and granular gel medium by their conformation [15].  
32 Among the bulk gel mediums, Pluronic [16-18], modified cellulose nanofibers [19-21],  
33 modified hyaluronic acid [22, 23], and Laponite [18, 24, 25] are commonly used. The  
34 embedding medium based on the Pluronic has a limited print window and weak  
35 recoverability, and the reported Pluronic-based medium has a high concentration which  
36 limits its biocompatibility. The modified cellulose nanofibers and hyaluronic acid  
37 require multi-step physical or chemical modifications, challenging the fabrication of  
38 large-scale structures. Laponite, as a type of inorganic colloid, is difficult to be removed  
39 and also decreases cell viability. The appearance of the granular gel medium broadens  
40 the range of material selection. Amid the granular mediums, the Carbopol [8, 26-28],  
41 gelatin microparticles [7, 9, 29], and agarose [13, 30] are widely used. However, their  
42 conformations make it difficult to provide controllable yield stress and to support the  
43 high precision printing [15]. Besides, the ionic sensitivity of Carbopol, the temperature  
44 sensitivity of gelatin microparticles, and the removal difficulty of agarose  
45 microparticles limit their biomedical applications. Therefore, considering the  
46  
47  
48  
49  
50  
51  
52  
53  
54  
55  
56  
57  
58  
59  
60

sensitivity of temperature, ion, pH changes, light, and enzyme, the removal difficulty, and the production difficulty, the current features of embedding mediums are too limited for the construction of multi-material well-defined tissue-like structures. To fulfill all these requirements, an ideal embedding medium should have controllable rheological properties, reasonable stability, excellent biocompatibility, versatility to support different bioinks, and ease of removal [7, 15, 31, 32].

In this paper, we proposed a novel hydrophobic interaction-based supporting medium, which has a tunable print window, compatibility with a majority of bioinks and crosslinkers, and a corresponding removal strategy to meet the aforementioned demands. This medium consists of two commercially available materials, hydrophobically modified hydroxypropylmethyl cellulose (H-HPMC, a biocompatible excipient (Type IV) approved by Food and Drug Administration (FDA)) and Pluronic F-127 (PF-127), which is termed as the HP embedding medium. The adjustable dynamic hydration permits the regulable rheological properties of the medium. The macromolecular backbones and hydrogen bonds make the medium hardly compromised by additives without strong hydrophilic groups, which makes multi-material printing requiring various crosslinking methods possible. The polyethylene glycol (PEG400) is used to decrease the medium viscosity as the removal bath because of its hydrophilicity. The stability of the medium and the printing precision of the freeform writing was investigated by analyzing the velocity field and filament features. Then we constructed tubular structures with different branching designs to evaluate the printing precision, the release process of the prints, and the biocompatibility of the medium. Finally, taking advantage of the versatility and ideal rheological properties, a multi-crosslinking printing method and a versatile enhanced adhesion writing method were introduced, which supports multi-crosslinked material printing in a single medium and enhances the adhesion between subsequently printed layers to solve intrinsic strength issues of the layer-by-layer fabrication. This medium extends the choice of the bioinks to lay the groundwork for multi-material heterogeneous organs/tissues biofabrication.

## 2. Materials and methods

### 2.1 Preparation of the embedding medium, the bioink, and the removal bath

The HP embedding medium is comprised of the PF-127 (Sigma-Aldrich, USA), and the H-HPMC (commercial name Sangelose 90L, Daido Chemical Co., Japan). The PF-127 powder was dissolved in  $1 \times$  phosphate buffer saline (all PBS used in the study are  $1 \times$  PBS) (GENOM, China) and stored overnight at 4 °C. The PF-127 solution was then heated to 47 °C under stirring. The H-HPMC powders were gradually added to the PF-127 solution at a speed of 800 rpm. Upon completing dissolution, the temperature of the mixture was then decreased to room temperature (RT, 26 °C) gradually while keeping continuous stirring. The cooled medium was then transferred into a translucent acrylic box prior to printing. To explore the influence of additives on medium

1  
2  
3  
4  
5  
6  
7  
8  
9  
10  
11  
12  
13  
14  
15  
16  
17  
18  
19  
20  
21  
22  
23  
24  
25  
26  
27  
28  
29  
30  
31  
32  
33  
34  
35  
36  
37  
38  
39  
40  
41  
42  
43  
44  
45  
46  
47  
48  
49  
50  
51  
52  
53  
54  
55  
56  
57  
58  
59  
60

rheological properties, 0.05%, 0.1%, 0.2%, and 0.4%  $\text{CaCl}_2$  were added to 10% PF-127/2.5% H-HPMC. Besides, 0.05%, 0.1%, 0.2%, and 0.4% NaOH, and 0.25%, 0.5%, 1%, and 2% GGT were added to 10% PF-127/3% H-HPMC medium, respectively. For multi-crosslinking printing, the PF-127 solution was supplemented with 0.1% (w/v)  $\text{CaCl}_2$  (SCR, China), 1% transglutaminase (GGT, Cool Chemistry, China), and 0.1%/0.05% NaOH (SCR, China) first and then mixed with H-HPMC.

For bioinks, a 10% (w/v) solution of gelatin from porcine skin (Sigma-Aldrich, USA) was prepared by dispersing the appropriate mass of gelatin in PBS and warmed to 37 °C, into which 0.1% (w/v) food dye or  $1 \times 10^6$  fluorescent beads/ml (2  $\mu\text{m}$  in diameter, Beiting, China) was added for the tracking purpose. The 5% (w/v) and the 15% (w/v) gelatin methacryloyl (GelMA GM-90, EFL, China) were dissolved in PBS with 0.5% (w/v) lithium phenyl-2,4,6-trimethylbenzoylphosphine (LAP, EFL, China) as the photoinitiator, and 0.1% (w/v) of food dye or  $1 \times 10^6$  fluorescent beads/ml. For the cytocompatibility experiments, GelMA was dissolved in the cell-culture medium instead of PBS. The 4% (w/v) sodium alginate powder and 0.1% (w/v) food dye or  $1 \times 10^6$  fluorescent beads/ml were dissolved thoroughly in PBS by stirring at 50 °C for 20 minutes at 600 r/min to form a sodium alginate solution. The 3.5% (w/v) chitosan solution and 0.1% (w/v) food dye were prepared by homogeneously dispersing the chitosan powder and the food dye in 2% (v/v) acetyl acid (SCR, China) at 800 r/min stirring for 20 minutes at 50 °C. In addition, the 1% (w/v) collagen (Corning, USA) was used.

Polyethylene glycol 400 (PEG400, SCR, China) was pre-mixed well with PF-127 solution at room temperature at 1%, 3%, and 5% (v/v) concentration to carry out rheological tests. The 5% (v/v) concentration solution was used as the removal bath for the supporting medium.

Sterilization procedures were taken into account for all the supporting medium, bioink, and removal bath introduced in this research. The PF-127, GelMA, PEG, and collagen solutions were filtered through a 0.22  $\mu\text{m}$  filter (Millipore, USA). And H-HPMC powders were sterilized by UV exposure for 30 minutes and then dissolved following the same procedure under sterile conditions.

## 2.2 Rheological measurements

The rheological measurements of the embedding medium were performed with a rotational rheometer (MCR102, Anton Paar, Austria) using a 1 mm gap and a parallel plate rotator with a diameter of 25 mm. Apparent viscosity was measured as a function of temperature with a fixed shear rate of  $1 \text{ s}^{-1}$ . The storage modulus ( $G'$ ) and loss modulus ( $G''$ ) were also measured as a function of temperature via oscillation tests at the oscillatory strain of 1% and frequency of 1 Hz. For all temperature sweeps, samples were loaded onto the test plate and heated to steady 40°C prior to the experimentation and then cooled from 40°C to 4°C with a ramp of  $-2 \text{ °C/min}$ . Shear rate sweeps were executed to evaluate the apparent viscosity as a function of shear rate at a logarithmic

sweep ( $0.001\text{--}100\text{ s}^{-1}$ ). Shear storage modulus and loss modulus were measured as a function of frequency via oscillation tests with a logarithmic sweep of frequencies ( $0.1\text{--}10\text{ Hz}$ ) at the oscillatory strain of 1%. Recoverability of samples was measured by recording the viscosity variations during 3 steps: (i) low shear rate ( $0.01\text{ s}^{-1}$ ) for 1 minute, (ii) high shear rate ( $10\text{ s}^{-1}$ ) for 10 seconds as a residence time when nozzle passed through the medium, and finally (iii) low shear rate ( $0.01\text{ s}^{-1}$ ) for 1 minute to trace the extent of recovery. The testing temperature was set to  $26^{\circ}\text{C}$  except for temperature sweep tests.

### 2.3 Particle imaging velocimetry (PIV) analysis of flow field

To visualize the flow field with PIV, fluorescent beads ( $2\text{ }\mu\text{m}$  in diameter, detected with a green laser of  $527\text{ nm}$ , Beiting, China) were mixed thoroughly with the HP embedding medium with the concentration of  $1 \times 10^7$  beads/ml. A transparent cubic container ( $30\text{ mm} \times 30\text{ mm} \times 30\text{ mm}$ ) filled with embedding medium prior to the PIV experiment was mounted to a linear motion platform to generate the movement. To capture the images during the nozzle translation, the apparatus was suspended over a high-speed camera (NOVA S12, Photron, Japan). To investigate the stability of the HP embedding medium, a set of experiments were carried out in an orthogonal manner. Nozzles with  $38\text{ mm}$  length and four different gauge sets were used (22, 23, 25, 27 gauges with  $0.68\text{ mm}$ ,  $0.59\text{ mm}$ ,  $0.48\text{ mm}$ , and  $0.37\text{ mm}$  outer diameter). The travel speeds were set at five levels ( $1\text{ mm/s}$ ,  $3\text{ mm/s}$ ,  $6\text{ mm/s}$ ,  $12\text{ mm/s}$ ,  $20\text{ mm/s}$ ). To keep the mean particle displacement within the range of 5 to 15 pixels, the frame rate for imaging was chosen to be 333 frames per second (fps) for  $20\text{ mm/s}$ , 200 fps for  $12\text{ mm/s}$ , 100 fps for  $6\text{ mm/s}$ , and 80 fps for other velocities [33]. The data were analyzed using the PIVlab module [34] with interrogation windows of  $64 \times 64$  pixels with 50% overlap for the coarse grid and  $32 \times 32$  pixels with 50% overlap for the refined grid system.

### 2.4 Printing protocols

A customized 3D bioprinter was produced comprising a temperature control module, a nozzle motion control module, and a bioink dispensing system, as we reported before [5]. Digital 3D models were designed using SolidWorks or downloaded from Thingiverse ([www.thingiverse.com](http://www.thingiverse.com)) (“Human right-hand” by dgo (modified), under the Creative Commons – Attribution license- CC BY 3.0 – <https://creativecommons.org/licenses/by/3.0/>; “DNA double helix” by Diegoso (modified), under the Creative Commons – Attribution license- CC BY 3.0 – <https://creativecommons.org/licenses/by/3.0/>; “Tetrahedron” by wouterglorieux (unmodified), under the Creative Commons – Attribution license- CC BY 3.0 – <https://creativecommons.org/licenses/by/3.0/>; “ZJU letters” by kresty (modified), under the Creative Commons – Attribution license- CC BY 3.0 – <https://creativecommons.org/licenses/by/3.0/>), and then sliced by Cura 4.7 to generate

the G-codes for printing. The generated G-codes were further reprogrammed using an R script to optimize the printing continuity. All printing experiments were performed within a transparent acrylic container (30 mm × 30 mm × 30 mm) filled with embedding medium to facilitate the light penetration. To exclude the influence of the container wall, the start height of printing was set as 3 mm higher than the container bottom.

To investigate the printing precision, the same nozzle set used in the PIV test was used to print filaments in the HP embedding medium. The printing pressures varied from 60 kPa to 220 kPa for different nozzles, with a 20 kPa adjustment step. And the velocity was set to 1 mm/s, 3 mm/s, 6 mm/s, 12 mm/s, and 20 mm/s respectively. Printed filaments were exposed to a blue light source (405 nm, 25 mW/cm<sup>2</sup>, 3 cm below the container bottom) to crosslink for 1.5 minutes and evaluated by inverted fluorescence microscopy (Leica DMiL, Leica, Germany). Diameter profiles of the filaments were measured nine times for each condition with Image J.

All the printed branching tubular structures were designed with a 4 mm outer diameter in this study. And 15% GelMA, 25G nozzles, 150 kPa extrusion pressure, and 6 mm/s velocity were adopted for all tubular structure printing processes. The printed structures were exposed to blue light for 1.5 minutes to crosslink. The printed structure and the surrounding medium were removed from the container with a spatula and then transferred to the removal bath under stirring. The residual medium inside the tube was fully discharged by pipetting the removal bath through the channels.

For the printing of the multi-crosslinked materials, the abovementioned bioinks were printed into the HP embedding medium with/without crosslinkers and then crosslinked separately or together. In brief, the 5% GelMA solution was printed in the 10% PF-127/3% H-HPMC medium at 24 °C, exposed to the blue light for three minutes followed by washing and removing to 37 °C PBS. The 10% gelatin solution was deposited into the 10% PF-127/3% H-HPMC medium at 27 °C, solidified in a 4 °C refrigerator for 30 minutes, followed by washing and releasing to 0 °C PBS. The 4% alginate solution was written into the 0.1% CaCl<sub>2</sub>/10% PF-127/2.5% H-HPMC medium, crosslinked for six hours, followed by washing and removing to RT PBS. The 10% gelatin solution was also printed in the 1% GGT/10% PF-127/3% H-HPMC at 27 °C, crosslinked for six hours, followed by washing and removing to 37 °C PBS. The 3.5% chitosan solution was printed in the 0.1% NaOH/10% PF-127/3% H-HPMC medium, crosslinked for six hours, and then washed and removed to RT PBS. The 1% (w/v) collagen was printed in the 0.05% NaOH/10% PF-127/2% H-HPMC medium at 4 °C, and then stored in 37 °C for 30 minutes to allow fibrillation, which was finally released from the bath to PBS at RT. The 5% GelMA, the 10% gelatin, and the 4% alginate were utilized together to construct letters and a triple-layer tube in the 1% GGT/0.1% CaCl<sub>2</sub>/10% PF-127/2.5% H-HPMC at 24 °C, 27 °C, and RT, respectively. They were then exposed to a blue light source for three minutes and crosslinked for six hours. Subsequently, post-crosslinked constructs were removed from the medium to 37 °C PBS. For all experiments, the embedding mediums were kept at RT.



We further developed a versatile post-printing method to enhance the adhesion between adjacent layers of the prints, adopting identical material and printing parameters. Briefly, the multi-crosslinked structures were printed in a layer-by-layer manner. The fabricated structures were captured in the embedding medium. The whole container was then transferred to a thermostat water bath and heated for 10 minutes at 33 °C before crosslinking and the removal of the embedding medium. Meanwhile, those in the control group were kept at room temperature (RT) for 10 minutes followed by crosslinking, removing, and washing.

## 2.5 Mechanical Characterization

Tensile properties of the fabricated tubular specimens were evaluated by uniaxial tests, with a universal testing machine (ElectroForce 3200, TA Instruments, America) at RT. According to ISO 7198, tubular specimens were opened longitudinally and laid flat to obtain rectangular samples. The specimens were then mounted on the grips of the testing machine. The uniaxial tensile test was performed with a constant ramp of 1 mm/min until the specimen failure happened. And the tensile properties were presented by the elastic modulus (strain below 0.1) and the maximum strain of the tubular specimens.

## 2.6 Cell culture and bioink preparation

Human umbilical vein endothelial cells (HUVECs, iCell, China) were cultured in T25 flasks with 5% fetal bovine serum (iCell, China), 1% penicillin-streptomycin (Life Technologies, USA), 1% endothelial growth factors (iCell, China), and 93% culture medium (iCell, China) under a 5% CO<sub>2</sub> concentration (Thermo, USA). This cell line was used at passage 6. The HUVECs were treated with Trypsin-EDTA (0.25%, Life Technologies, USA), centrifuged at 1,000 r/min, and then gently mixed into the GelMA solution at 37°C before loading into syringes. The typical final concentrations of each component were as follows: 15% GelMA, and ca.  $3 \times 10^6$  cells/ml.

## 2.7 Fluorescence Staining and Microscopy

In the shape fidelity study of the printed structure, the wall thickness, lumen diameter, and outer diameter were measured by fluorescence microscopy (Leica M165 FC, Leica, Germany). To visualize fluid flow through bifurcated tubular structures, fluorescent beads ( $1 \times 10^6$  beads/ml) were dispersed in PBS and injected into the tube using a small syringe. The flow field was then detected on fluorescence microscopy (Leica M165 FC, Leica, Germany). For the perfusion demonstration of two complex tubular structures, dark food dye was diluted in PBS and injected into the tube using a syringe pump. The perfusion process was recorded at 30 fps in S.I. media.

For the cell-laden specimens, the experimental group was deposited in the medium and the control group was deposited in the air. The structures were fabricated and cultured in tubular form, then opened longitudinally, and laid flat, prior to the

observation. For the Live/Dead staining experiment, a Live/Dead cell viability/cytotoxicity assay kit (Thermo, USA) was used to determine cells' viability on day 1, day 4, day 7, and day 10, respectively. The assay solution was prepared by mixing 1  $\mu$ l/ml Cal-AM and 2  $\mu$ l/ml propidium iodide in PBS. Then, the mixture was added to the samples and incubated for 30 min. After three 3-min washes with PBS, the samples were evaluated using fluorescence microscopy (Leica M165 FC, Leica, Germany). For each sample, three fluorescent images were obtained from different areas. Live cells were shown in green, while dead cells were shown in red. The number of live and dead cells was counted using ImageJ (NIH, USA) software. Cell viability was calculated as the counts of living cells divided by the total cell counts.

To evaluate the cell growth during the culture process, F-actin/4',6-diamidino-2-phenylindole (DAPI) staining was carried out. Printed structures were fixed with 4% paraformaldehyde (Cyagen, China) for 30 minutes, and permeabilized using 0.1% Triton X-100 (Amresco, USA) in PBS for three min. Upon permeabilization, the samples were thoroughly washed with PBS. The samples were then stained with TRITC Phalloidin solution (80 nM, Fushen, China) for 30 minutes, followed by DAPI solution (0.5  $\mu$ g/ml, Solarbio, China) for another 15 minutes. The samples were then opened longitudinally, laid flat, and observed by fluorescence microscopy (Leica M165 FC, Leica, Germany). For each sample, three fluorescent images were obtained from different areas. Cell nuclei were shown in blue, while the F-actin was shown in red. The number of cells was quantified using ImageJ (NIH, USA) software according to the number of cell nuclei. All images were randomly taken on the surface of three replicates, processed in ImageJ, and one representative image was presented.

2.8 Statistical analysis

Continuous variables were checked for normality and log-transformed if necessary. Two-group comparisons were made using student's t-test, and multiple-group comparisons were made using one-way analysis of variance (ANOVA) in conjunction with Tukey's test for post hoc analysis. All analyses were performed using the "R" statistical package using R-Studio v 1.4.1103. All continuous data were presented as mean  $\pm$  standard deviation (S.D.). The P values were provided and significance levels are as follows: \* $p < 0.05$ , \*\* $p < 0.01$ , \*\*\* $p < 0.001$ , \*\*\*\* $p < 0.0001$ .  $n \geq 3$  for printing precision experiment and enhanced adhesion writing experiment, and  $n \geq 9$  for cytocompatibility experiment.

3. Results and discussion

3.1 Rheological properties of the HP embedding medium

We propose a new solution to the existing problems of current embedding mediums, utilizing the hydrophobic association between H-HPMC and PF-127 (figure 1). H-HPMC contains grafted hydrophobic stearyl groups to cellulose backbone. This cellulose derivative is an excipient (Type IV) approved by FDA, and its safety and

hydrophobicity properties have been previously discussed [35, 36]. PF-127 is a type of triblock copolymer of poly(ethylene oxide) and poly(propylene oxide) in a PEO-PPO-PEO configuration, which shows hydrophobicity through its PPO blocks in the mid-chain, and hydrophilicity with the PEO blocks on each side [37].

In aqueous dispersion below the critical micellization concentration, the PPO blocks on PF-127 tend to assemble around the stearyl group of H-HPMC due to strong hydrophobic association, as illustrated in figure 1. In this case, the entanglement in the embedding medium would be a combination of inter-chain and intra-chain entanglement of the HPMC chain and PEO end blocks. Therefore, in a static situation, the medium demonstrates solid-like behavior with relatively high viscosity. Once a nozzle passes, shear stress is applied to the surrounding medium, and the polymer chains would progressively disentangle and elongate, resulting in a descending viscosity, which is termed the shear-thinning property [38] (figure 1A (i)). The liquified region allows a cell-contained bioink to flow out of the nozzle (figure 1A (ii)). After

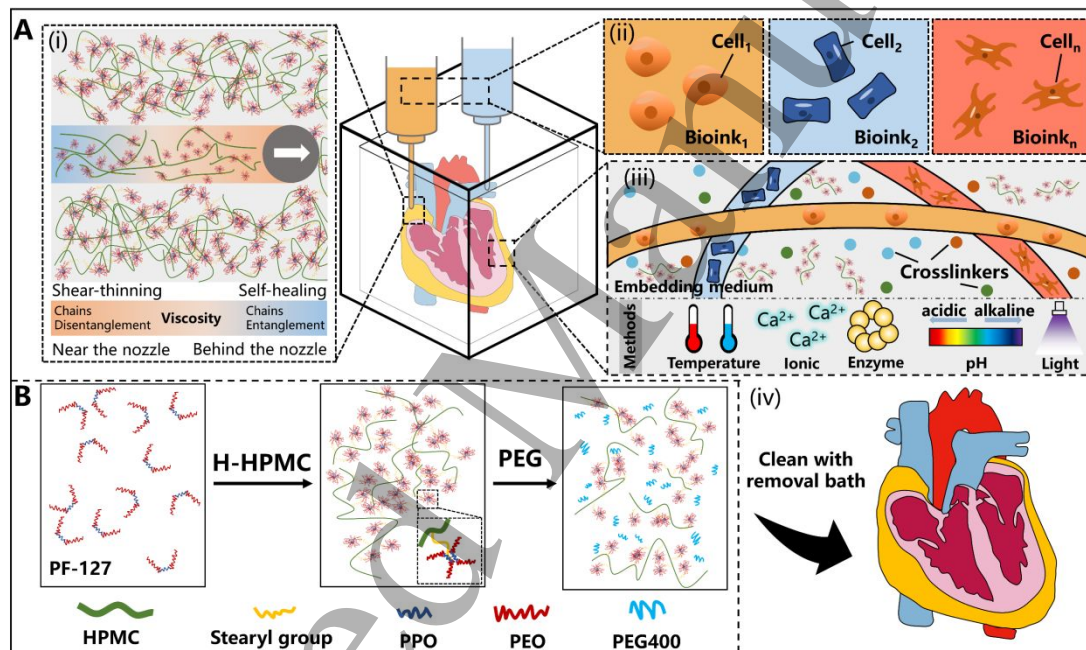


**Figure 1. Freeform writing in the HP embedding medium.** (A) An illustration of the extrusion of bioink into the HP embedding medium to write a complex pattern. (i) The medium is composed of H-HPMC and PF-127, fluidizes when stress is applied by the displacement of nozzle (red region), and recovers by its self-healing properties (blue region). The medium that does not withstand shear stress is providing global stability for the written pattern (grey region). (ii) The different cell-laden bioinks are deposited into the liquified region with multiple nozzles and kept in situ (iii). (iv) The embedding medium could be removed to obtain a structure suitable for further applications. (B) A schematic representation of the HP embedding medium. With PEG400 added, the association between hydrophilic PEO blocks of PF-127 was decreased, thus decreasing the viscosity for the ease of removal.

removing the applied shear stress, the reconstruction of chain associations recovers the viscosity of the medium, showing its self-healing property. The printed bioink is therefore kept in situ. The cellulose backbone and the hydrogen bonds make the medium stable in many crosslinking conditions, including temperature, ion, enzyme, light, and a range of pH values. With embedded crosslinkers, the deposited bioink could be cured or crosslinked to form an intact structure (figure 1A (iii)). Finally, the medium was removed to obtain a structure suitable for further application (figure 1A (iv)). With these characteristics, the proposed solution is a potential versatile embedding medium, which could provide suitable printing conditions for a large variety of bioinks with different crosslinking methods.

The hydrogen bonds are affected by additives with different hydrophilic functional groups [17, 39]. Accordingly, PEG400, a small biocompatible homopolymer with hydrophilicity, was used to regulate the medium viscosity (figure 1B). It is a kind of polymer approved by the FDA for use in drug delivery systems [40]. Although PEG400 has a small molecular weight, its biocompatibility has been identified in previous studies [40]. Compared with cells incubated in PEG1000 and PEG4000, cells incubated in PEG400 solutions for 24 hours showed pronouncedly higher viability [41]. Therefore, it might serve as a biocompatible material used in the freeform writing process. It could interpose between macromolecular backbones to decrease the overall viscosity, making it possible to remove the printed structures from the embedding medium without integrity jeopardy [42].

Rheological tests were carried out to manifest and understand the effect of each component on the final properties of the embedding medium, including temperature sweep, shear rate sweep, thixotropy test, and frequency sweep [6] (figure 2, figure S1). In this section, H-HPMC (2%, 3% and 4% w/v) and PF-127 (5%, 10% and 15% w/v) were chosen in the tests, where the formation of gel was feasible.

The addition of the H-HPMC concentration enhanced the overall solution viscosity monotonically within the tested temperature range (20-30 °C, figure 2A), whereas the influence of the PF-127 concentration was different. A low concentration of PF-127 (5%) made the embedding medium almost temperature insensitive. In contrast, a high concentration (15%) of PF-127 resulted in an ultra-high medium viscosity and showed a sharp rise when the temperature increased. Shear rate sweep results were used to demonstrate the shear-thinning property of the medium and showed results similar to the temperature sweeps (figure 1B, table 1). The results were fitted with the Herschel-Bulkley model (HB), which is expressed as follows:

$$\sigma = \tau_y + k\dot{\gamma}^n, \quad (1)$$

where  $\sigma$  is the shear stress,  $\tau_y$  is the yield stress,  $\dot{\gamma}$  is the shear rate,  $k$  is the flow consistency index, and  $n$  is the flow behavior index. The yield stress  $\tau_y$ , one of the most important parameters during the embedded bioprinting, could be regulated from 0.59 Pa to 91.11 Pa for different combinations of concentration. It increased monotonically with the H-HPMC concentration, and it was also dramatically affected by the PF-127

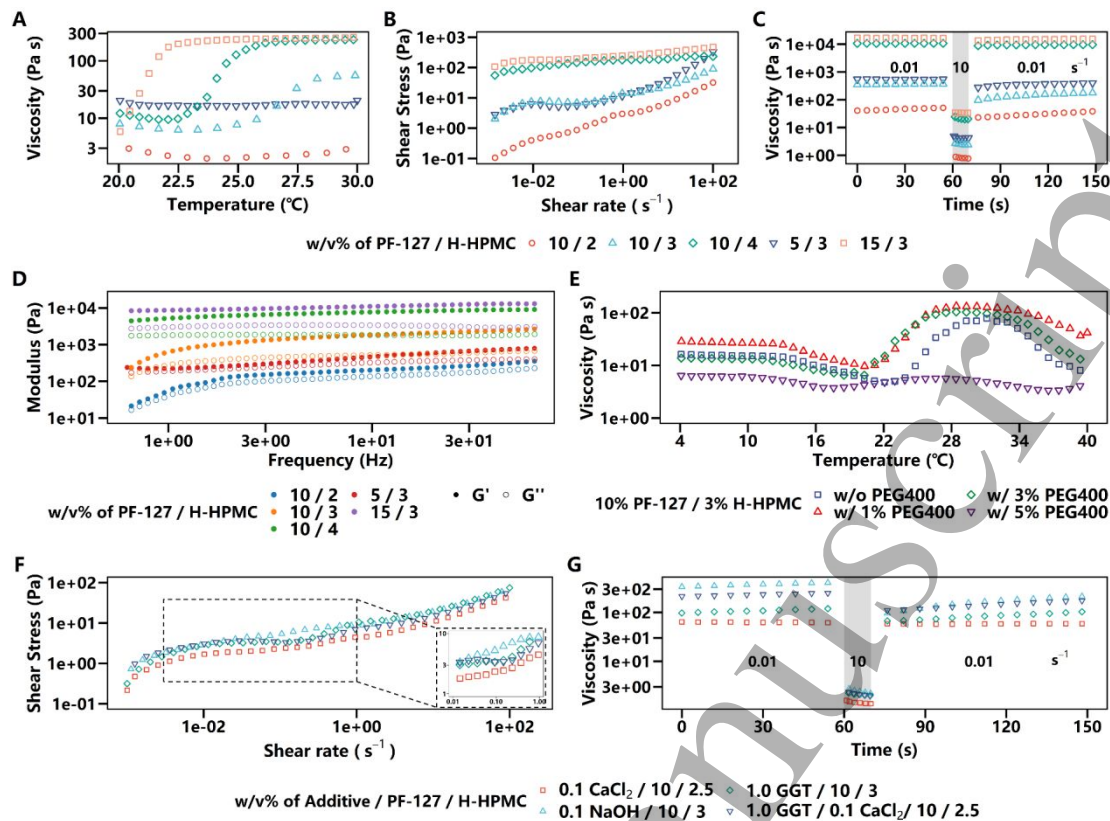


**Figure 2. Rheological characterization of the HP embedding medium.** (A-D) The influence of the H-HPMC and PF-127 concentration on the (A) temperature sweep, (B) shear rate sweep, (C) thixotropy test, and (D) frequency sweep. (E) The influence of temperature and PEG400 additive on the HP embedding medium. (F-G) The influence of additives on the HP embedding medium, including 0.1% CaCl<sub>2</sub>, 0.1% NaOH, 1% GGT, and 1% GGT with 0.1% CaCl<sub>2</sub>. (F) The shear rate sweep of the 10% PF-127/3% H-HPMC embedding medium containing different additives. All samples show shear-thinning properties and have yield stress. Inset: yield area of the medium. (G) The thixotropy test for samples with different additives. The self-recoverability and fast thixotropic response time are observed amid the samples. All the tests, in addition to temperature sweep tests, are carried out at room temperature (26 °C).

concentration. These phenomena might attribute to the combination of components. H-HPMC is a type of hydrophobic polymer, whose stearyl groups tend to assemble with each other, showing high viscosity and temperature insensitivity (figure S2) [35]. After adding PF-127, PPO groups of PF-127 would hydrophobically associate with stearyl groups of H-HPMC, forming a compact core that was surrounded by PEO blocks. Therefore, the bath showed PEO blocks dominated fluid behaviors. However, even though the H-HPMC assembles PF-127 to increase the local concentration of PEO blocks, insufficient PF-127 concentration (5%) would still not lead to PEO blocks entanglement, which made the viscosity of the bath not change with the temperature. Besides, PPO blocks would associate with a part of stearyl groups, resulting in a decreased medium viscosity. After raising the PF-127 concentration (10%), more

**Table 1. The yield stress and the thixotropic time of the embedding medium with different concentrations (w/v)**

PF-127	H-HPMC	Additives	Yield Stress (Pa)	Thixotropic time (s) <sup>a)</sup>
5	3	-	6.45	< 3
10	2	-	0.59	< 3
10	2.5	-	2.33	< 3
10	3	-	5.89	< 3
10	3.5	-	45.07	< 3
10	4	-	76.38	< 3
15	3	-	91.11	< 3
10	2.5	0.1% CaCl <sub>2</sub>	2.45	< 3
10	3	1% GGT	2.55	< 3
10	2	0.05% NaOH	0.57	< 3
10	3	0.1% NaOH	3.78	< 3
10	2.5	1% GGT, 0.1% CaCl <sub>2</sub>	3.49	< 3

<sup>a)</sup> The time point when the viscosity recovers to 50% of its original viscosity is regarded as the Thixotropic time

stearyl groups would be associated, leading to a concomitant decrease of viscosity in low temperatures. Meanwhile, the increased PEO group concentration would result in inter-chain entanglement in high temperatures, enhancing the medium viscosity. On the other hand, further improving PF-127 concentration (15%) would dramatically improve the local concentration of PEO groups, making them easier to entangle with each other. It made the viscosity of the medium improve pronouncedly in relatively low temperatures. Also, based on this principle, a critical ratio between the H-HPMC concentration and the PF-127 concentration might exist. The critical value was calculated to be 0.32, which was determined via experimental iterations (supporting information, figure S3). Thus, mediums with similar rheological properties could be obtained by adjusting the concentration of two components. For example, the 15% PF-127/3% H-HPMC medium and the 10% PF-127/4% H-HPMC medium showed similar rheological properties in high temperatures but responded differently in lower temperatures (figure 2A-C). Thixotropy tests confirmed a decrease of the medium viscosity under a high shear rate ( $10\text{ s}^{-1}$ ) and an immediate recovery after removing the load ( $0.01\text{ s}^{-1}$ ), which is the evidence of the shear-thinning and self-healing properties of the medium (figure 2C, table 1). The recovery time (recover to 50% initial viscosity) was found to be less than three seconds for all mediums, showing great self-



recoverability. The dynamic rheology measurement identified that the storage modulus  $G'$  was always greater than the loss modulus  $G''$ , implicating the medium was dominantly gel-like (figure 2D). Collectively, the HP embedding medium gained controllable rheological properties by regulating component concentrations, while its thermoresponsive could be tuned independently.

To explore the impact of PEG400 on the HP embedding medium, temperature sweeps were carried out at the 10% PF-127/3% H-HPMC medium without or with 1%, 3%, and 5% PEG400 (figure 2E). It was found that a small amount of PEG400 facilitated inter-chain entanglement due to its hydrophilicity, thus enhancing the viscosity HP-embedding medium. This phenomenon might be related to the presence of hydrophilic parts of PEG400 (oxygen atoms). They could be involved in interaction with water through hydrogen bonds, leading to a decrease of water molecules available to hydrate PEO blocks [17]. The increased local PEO block concentration could facilitate their inter-chain entanglements, which further enhanced the medium viscosity. Whereas a loss of temperature sensitivity of the mixture with more PEG400, reveals the disentanglement between chains through the plasticizer effects of hydrated PEG400 molecules [17], leading to the low viscosity of the composited medium (less than 3 Pa s), which significantly facilitates the removal of the embedding medium. In addition, crosslinkers were added to verify its versatility for different kinds of crosslinking strategies. We added  $\text{CaCl}_2$  (0.05%-0.4%), NaOH (0.05%-0.4%), and GGT (0.25%-2%) into the embedding mediums. It was found that the addition of additives did not eliminate the yielding, shear-thinning and self-healing properties of the embedding mediums (figure 2F-G, figure S4, table S1). The addition of  $\text{CaCl}_2$  potentially reduced the water activity of the system [43], which increased the polymer concentration to strengthen the viscosity of the medium. Whereas, the improvement of medium viscosity could be compensated by reducing the H-HPMC concentration. And other additives almost did not affect the rheological properties of the embedding medium except for the effect of dilution because of their neglectable influences on hydrogen bonds between PEO blocks and water molecules, and macromolecular backbones [44, 45].

Numerous bulk gel and granular gel baths have been applied in embedded printing. However, they could be salt-unstable (Laponite [18, 24, 25], Carbopol [8, 26-28]), temperature-unstable (gelatin [7, 9, 29], agarose [13, 30], gellan [31]), complex-modification required (modified hyaluronic acid [22, 23], modified cellulose nanocrystals [21]), difficult to remove (cellulose nanocrystals [46], Carbopol), or biological incompatible (diblock and triblock copolymers [10]). Herein, we advance the embedding medium by combining biocompatible H-HPMC and PF-127 to form a hydrophobic interaction-based medium, owning adjustable rheological properties, versatility on printing, and crosslinking conditions, easy-removal property, and biocompatibility. Those characteristics lay the groundwork for multi-material heterogeneous organs/tissues biofabrication.

### 3.2 Stability of the Freeform Writing in the HP embedding medium and the printing resolution

When a nozzle passes through, a velocity field is generated that may have effects on the printed structures within the range and result in a loss of shape fidelity. The medium stability is thus defined as the ability to keep its shape against the shear stress, specifically when a nozzle moves within the medium. Though the HP embedding mediums have a high elastic modulus, proper yield stress, and fast thixotropic time to keep stable [47], the rheological tests cannot simulate the full-scaled printing process. Therefore, to understand the deformation of the embedding medium during the freeform writing, and to optimize the embedding medium compound, we performed the PIV analysis using variable concentration mediums and different printing parameters.

To simulate the freeform writing in the medium, an acrylic box filled with the embedding medium was translated relative to a stationary tip (figure 3A), the medium was loaded with fluorescent beads, so the velocity field can be tracked with a high-speed camera, and analyzed by PIV package. Colored contours were used to display the magnitude of the velocity for different mediums (figure 3D-F). The nozzle movement resulted in a disturbance of the velocity field around the nozzle, which became stronger with decreasing yield stress. The most affected area was along the moving direction (X-axis). When the nozzle passed, the tip would compress the medium forward and drag the medium behind, leading to vortices [33], and this direction was the most concerned by previous literature [8, 20, 24]. However, the concomitant tangential force would apply shear stress to the medium normal to the moving direction (Y-axis). The disturbance along the Y direction might push/pull the deposited structure, resulting in a loss of shape fidelity, which should not be neglected. Quantitative analysis was conducted for each individual situation (figure 3B-C, figure S5-S6). Normalized lengths ( $L_n$ ) and velocities ( $v_n$ ) are used to evaluate the range and amplitude of the disturbance, which can be calculated as follows:

$$L_n = \frac{l}{D}, \quad (2)$$

$$v_n = \frac{u - U}{U}, \quad (3)$$

where  $l$  is the distance from the nozzle,  $D$  is the nozzle outer diameter,  $u$  is the local velocity, and  $U$  is the moving velocity. Exponential decay of normalized velocity was found in every direction (X+, X-, and Y). The affected region was limited to twice the nozzle outer diameter. Beyond this range, the normalized velocity, representing the disturbance caused by the movement, decreased to less than 0.1. Comparing the collapsed curves of each individual group, faster exponential decay of velocity in all directions was observed with increasing yield stress. However, changes in other parameters, such as velocity magnitude and nozzle diameter, did not affect the exponential decay (figure S5-S6). The same observation was also identified by previous literature [8, 24]. The velocity and the nozzle diameter affected the maximum disturbance range rather than the convergence rate [33]. Their influences appeared



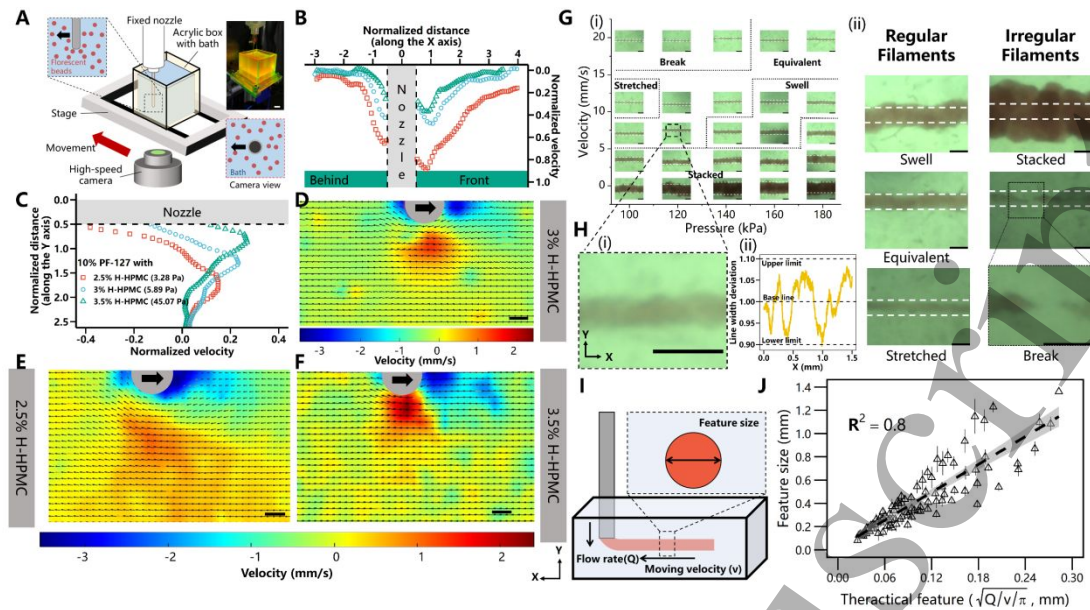


**Figure 3. Stability characterization of the HP embedding medium and the control of written features.** (A) Schematic view of the PIV experimental set-up. A 1D motion-controlled stage with a fixed nozzle is installed above a high-speed camera. (B) Normalized velocity  $v_n$  vs. distance  $Ln$  along and (C) normal to the moving direction  $X$  within the medium. (D) Representative velocity contour with velocity vectors of the 10% PF-127/3% H-HPMC medium. (E) Representative velocity contour with velocity vectors of the 10% PF-127/2.5% H-HPMC medium. (F) Representative velocity contour with velocity vectors of the 10% PF-127/3.5% H-HPMC medium. (D)-(F) 25G nozzle (outer diameter = 0.51 mm) and 6 mm/s velocity were used. (G) (i) A typical two-dimensional phase diagram shows the influence of velocity and pressure on the feature size, using a 25G nozzle (inner diameter = 0.25 mm) and the 10% PF-127/3% H-HPMC medium. (ii) Representative images of five types of filaments. (H) (i) An equivalent-diameter filament and (ii) its line width deviation. (I) An schematic of the feature size. (J) The feature size of printed lines could be controlled by regulating the flow rate of the ink through the nozzle ( $Q$ ) and the velocity of the nozzle ( $v$ ) ( $n = 9$ ,  $p < 0.0001$ ). (Scale bars: (D-F) 200  $\mu\text{m}$ , (G) 400  $\mu\text{m}$ , (H) 500  $\mu\text{m}$ , data are plotted as mean  $\pm$  S.D.)

within two to five-fold the normalized length, where the normalized velocity was so small as to be neglected. Therefore, the influence of velocity and the nozzle diameter could be ignored.

The freeform writing precision in the embedding medium was evaluated by the resolution and the width deviation of the printed strands, therefore filament diameters were selected as featured size [8, 10, 19, 21, 48]. With different parameters, five types of filaments were observed during the writing process, termed as well-defined swollen filament, equivalent-diameter filament, stretched filament, broken filament, and stacked filament (figure 3G). The line width deviations of the equivalent-diameter

filament were measured (figure 3H (i)), whose maximum deviation was within 10% (figure 3H (ii)). The level of the deviation gained from the deposited filaments enables straightforward production of structures with great shape fidelity. We then quantified the resolution of freeform writing (figure 3I-J). It is demonstrated that the printed feature followed simple conservation of volume equation, which could be expressed as:

$$A = \frac{Q}{v} \quad (4)$$

where  $A$  is the feature's cross-section error,  $Q$  is the flow rate (supporting information), and  $v$  is the nozzle moving velocity (figure 3J). The deviation of the slope might attribute to the calculation of the flow rate by printing pressure. Following the equation, features between 100  $\mu\text{m}$  to 1000  $\mu\text{m}$  could be created.

In this section, we identified the stability of this embedding medium and the printing precision of the freeform writing in the proposed embedding medium. The experimental result has shown great stability, low deviation, and controllable printing resolution of the printed strands, which indicates a high level of printing precision is achievable via this method.

### 3.3 Freeform Writing of Complex Branching Tubular Structures

In this section, we further utilized the freeform writing method to print tubular structures in the medium, with different branching designs. The tubes were fabricated with cell-laden bioink, in which HUVECs were encapsulated in GelMA solution to explore biocompatibility. As the control group, cell-laden cylindrical tubes were printed in air. After the tubes were crosslinked, they were cultured for another 10 days to investigate the impact of the embedding printing procedure on living cells. Considering its appropriate yield stress, stability, and self-healing speed, the embedding medium used in this section contains 10% PF-127 and 3% H-HPMC. The 15% w/v GelMA was used to keep the tubular shape of printed structures in the air.

To evaluate the shape fidelity of the printed structure, four designs were printed, including two bifurcated tubes with different featured angles, a single-input-single-output vascular tree, and a single input four outputs two-stage tree. After freeform writing in the HP embedding medium, the fabricated tubes were photo-crosslinked and removed from the embedding medium to the removal bath under constant stirring. (figure 4A, movie S1-S2). The comparison of the featured angles between the CAD design and printed structure measurements was of major interest, as they would not be affected by the swelling or dehydration induced by the measuring process [31]. Detailed morphology analysis comparing the 3D model and the printed tubes was conducted according to the bright-field and fluorescent images (figure 4F, figure 4H-I, and figure S7). The featured angles are listed in table 2. For the simple branched prints, the maximum variation between the designs and measurements is 4.23%. The branched tubes were then perfused with fluorescent beads solution and shown to be capable of splitting fluid flow. Also, the washed vascular tree constructs were perfused with black

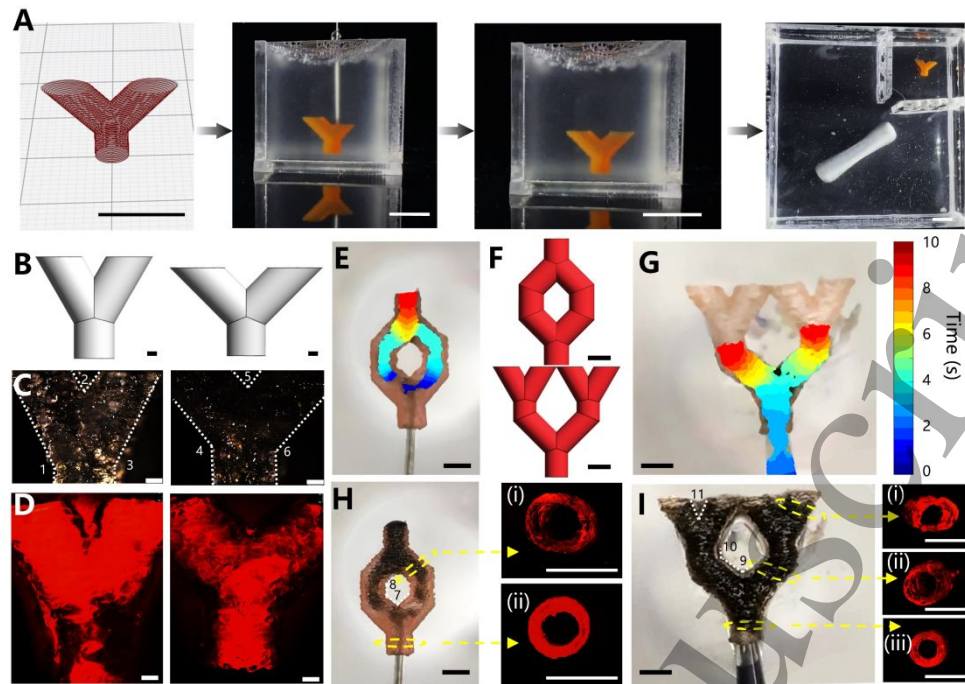


**Figure 4. Representative complex tubular structures printed in the HP embedding medium.** (A) An illustration of the process for fabricating complex structures. (B) CAD models of two bifurcated tubes with (left) 150°, and (right) 90° characteristic angles. (C) Bright-field images of the fabricated bifurcated tubes. (D) Fluorescent images of hollow tubes filled with fluorescent beads. (E) A time-lapse image of black dye perfused through the single-input-single-output vascular tree at time points of 0 to 10 s to show flow through the lumen. (F) CAD models of the (up) single-input-single-output vascular tree and (bottom) the single input four outputs two-stage tree. (G) A time-lapse image of black dye perfused through the single input four outputs two-stage tree at time points of 0 to 10 s to show flow through the lumen. (H) Bright-field images of the single-input-single-output vascular tree. Florescent cross-section images of the (i) convergence and the (ii) branch part. (I) Bright-field images of the single input four outputs two-stage tree and florescent cross-section images at the (i) inlet, the (ii) first branch, and (iii) the second branch part. (Scale bars: (A) 10 mm, (B)-(D) 1 mm, (E)-(I) 4 mm)

**Table 2. The designed and measured featured angles values**

Angle	1	2	3	4	5	6	7	8	9	10	11
Structure	Bifurcated tubes						Vascular trees				
Design	150.	59.6	150.	135.	89.8	135.	90.	134.	89.8	134.	62.5
(°)	78	7	78	30	1	30	59	86	1	86	3
Measure	153.	60.0	153.	141.	89.3	138.	94.	130.	90.3	135.	64.5
(°)	65	3	21	03	6	09	69	07	3	64	3
Error	1.90	0.60	1.61	4.23	0.50	2.0	4.5	3.55	0.57	0.58	3.20
(%)							2				

dye solutions as proof of their structural integrity (Figure 4E-I, Movie S3). The result shows that, with a higher level of complexity, the printed structure can still keep seamlessness and no significant leakage is observed. Due to the nature of this soft material used in the fabrication, the featured angle differences for vascular tree prints were relatively larger than the simple branches (up to 4.52%).

The freeform writing in the embedding medium is required to offer proper cytocompatibility for living cells during the writing process. Although the materials applied in the freeform writing, including H-HPMC, PF-127, PEG400, and GelMA are biocompatible and thus widely used in medical applications [16, 21, 46, 49], the impact of the entire freeform writing protocol on living cells needs to be further evaluated. In this experiment,  $3 \times 10^6/\text{ml}$  HUVECs were encapsulated in the bioink, deposited into the HP embedding medium and in air, respectively, to form tubular structures, and subsequently cultured for 10 days in vitro (figure 5). To keep tubular structure fidelity in the air and to directly compare the differences between freeform writing and printing in the air, we utilized 15% GelMA as the bioink. This concentration was also commonly used in bioprinting [50, 51]. The wall thickness of the fabricated tubes was controlled at around 400  $\mu\text{m}$  to guarantee cell viability, which is the critical distance to ensure the oxygen and nutrition transformation without micro-vessels [52]. Samples of the experimental group were in good shape of cylinders, while samples of the control group were found to collapse inwards as the cone and lose their shape fidelity. There was no statistical difference between the conventional printing controls and freeform writing groups in cell viability, which remained high ( $>85\%$ ) in 10 days of culture ( $n = 9$ , figure 5A, figure 5C, and figure S8). F-actin and DAPI staining demonstrated the proliferative capability of HUVECs in GelMA constructs for both groups, the results are shown in figure 5B and figure S9. The nucleus counting was adopted to reflect the proliferation ability of the deposited cells [53], which showed a significant increment, suggesting that cells could proliferate inside the printed tubes (figure 5D). It is noted that cells contained in tubular structures aggregated with each other, forming small clusters rather than interconnecting. It might attribute to the high stiffness and high network density provided by the 15% GelMA, which hinders the ability of cells to digest the surrounding hydrogel to create more space for cell interconnecting [50, 54]. Correspondingly, on the surface of the structure and in the low-concentration GelMA, cells could spread successfully to interconnect with each other after long-term culture (figure S10-S11). Finally, to evaluate the long-term shape stability of printed constructs, we compared the features of tubular structures undergoing long-term culture and the features of structures without culture (figure S11). In this experiment, 15% GelMA and 7% GelMA were used. For high concentration GelMA (15%), no significant difference was found between samples on day 0 and samples on day 14, concerning the wall thickness, inner diameter, outer diameter, and aspect ratio of cross-sections. However, for the low concentration GelMA (7%), significant changes in morphology and featured angles were observed. These observations might attribute to the impact of cells on bioinks that



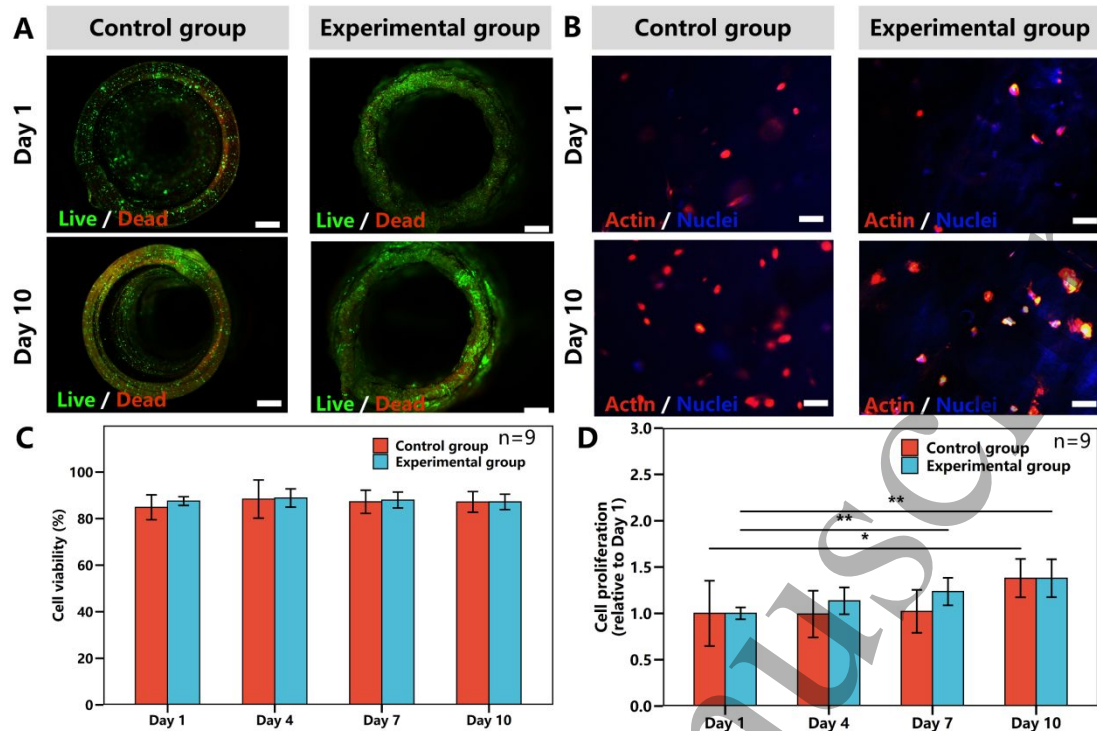


**Figure 5. Cytocompatibility of HUVECs laden tubular structures fabricated by freeform writing in the HP embedding medium.** (A) Representative Live/Dead staining images of cells encapsulated in the fabricated tubes and cultured for 1 and 10 days. (B) Representative F-actin/DAPI stained images of HUVECs encapsulated in the fabricated tubes and cultured for 1 and 10 days. (C) Quantification of cell viability from Live/Dead images (n = 9, p > 0.05). (D) Quantification of cell number per square millimeter counted from F-actin/DAPI staining images (n = 9, \* = p < 0.05; \*\* = p < 0.01). (Scale bars: A: 250  $\mu$ m, B: 50  $\mu$ m. Data are plotted as mean  $\pm$  S.D.).

cells would digest the soft GelMA (7%) to interconnect with each other, which would jeopardize the shape fidelity. However, it made the encapsulated HUVECs show CD31 successfully. On the other hand, the hard GelMA (15%) would inhibit the digestion to hold the shape features. Because the initial shape of all tubes was kept the same by freeform writing and no significant decrease in cell viability was observed in the first three days, the influence of freeform writing on long-term shape stability could be neglected [55]. Therefore, to acquire functionalized structures, it is necessary to balance the cell proliferation and shape maintenance in long-term culture by selecting appropriate bioinks. Overall, compared with the control group, the cytocompatibility of the HP embedding medium is reasonably good and this fabrication protocol has minimal impact on the living cells.

Collectively, these experiments have shown that the freeform writing in the HP embedding medium could be employed to print complex tubular structures with great biocompatibility. The manufacturing of tubes with reasonable aspect ratios, small diameter lumens, and hanging structures was successfully demonstrated, which is

impossible for conventional extrusion-based bioprinting. The injected fluids were successfully distributed throughout the entire structure, showing that the majority of the residual embedding medium was removed from the channel. It indicated the easy-removal property of the proposed embedding medium. Furthermore, lumens with about 2.6 mm inner diameters and about 4 mm outer diameter were constructed, showing the potential of the method to be applied in biomedical applications, especially for small-diameter vessel fabrication [56, 57].

*3.4 Freeform Writing in the Versatile HP Embedding Medium with Multi-crosslinking Methods*

Human organs/tissues are heterogeneous. For example, the internal and external elastic membranes of the blood vessel are composed of elastin, while its media and adventitia contain collagen, proteoglycans, elastin, and glycosaminoglycan [56]. Multi-material printing is always one of the major objectives for biofabrication. Though previous literature has explored some multi-material printing methods [58-60], the adopted materials were crosslinked by the same method at a time, such as the photo-crosslinking method, which has limited the bioink selection of the multi-material printing. The HP embedding medium we propose is a strong candidate to address this limitation. It is compatible with various additives, facilitating multi-crosslinked materials fabrication (figure 6A). The concentration of each medium component is determined by the yield stress and thixotropic time (table 1, and table S1) and preferred crosslinking time [31]. Printing demonstrations of several widely used bioinks corresponding to different crosslinking methods were presented (movie S4).

The supportive ability of the medium was first evaluated by non-additive assistant crosslinking methods, namely, photo-crosslinking and temperature-crosslinking. We adopted the 5% GelMA solution to fabricate a butterfly model in the 10% PF-127/3% H-HPMC medium. It was then crosslinked with a blue light source for three minutes and released from the medium. It was transferred into 37 °C PBS and showed good structure integrity (figure 6B). The 10% gelatin solution was used to construct a jellyfish model in the same medium. The medium containing the jellyfish was placed in a 4 °C refrigerator to solidify the bioink. After solidification, the jellyfish model was removed from the medium and placed into 0 °C PBS (figure 6C). We found the structure was comparable in size and included all the features presented within the original CAD model. We next demonstrated the capability of the embedding medium to promote the construction of materials crosslinked by enzyme, ion, and pH change. We created a DNA double helix structure out of 10% gelatin solution in the 1% GGT/10% PF-127/3% H-HPMC medium. With the existence of the enzyme, it was crosslinked after being kept for six hours. The structure was then removed from the medium and immersed into 37 °C PBS (figure 6D), which kept the shape fidelity under gentle agitation (movie S5). A right-hand model was then prototyped using the 4% alginate

solution, a material crosslinked by divalent cations, in the 0.1%  $\text{CaCl}_2$ /10% PF-127/2.5% H-HPMC

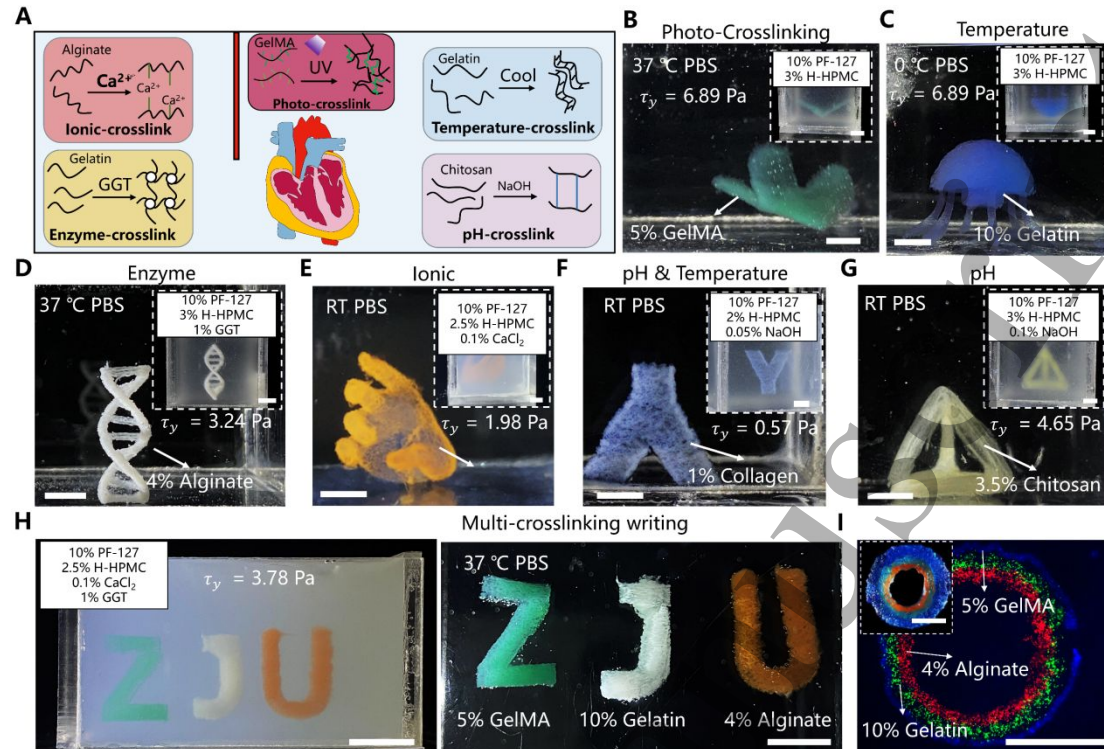


**Figure 6. The HP embedding medium as a versatile supporting bath material for extrusion printing.** (A) A schematic diagram of the versatile HP embedding medium applicable in various crosslinking strategies. (B) A butterfly composed of 5% GelMA was printed in the 10% PF-127/3% H-HPMC embedding medium, crosslinked by a blue light source, and removed to 37 °C PBS. (C) A jellyfish composed of 10% gelatin was written in the same medium, reversibly crosslinked by temperature, and removed to 0 °C PBS. (D) A DNA structure composed of 10% gelatin was constructed in the 10% PF-127/3% H-HPMC/1% GGT embedding medium, irreversibly crosslinked by transglutaminase, and removed to 37 °C PBS. (E) A hand composed of 4% alginate was deposited in the 10% PF-127/2.5% H-HPMC/0.1%  $\text{CaCl}_2$  embedding medium, crosslinked by  $\text{Ca}^{2+}$ , and removed to RT PBS. (F) A bifurcated tube composed of 1% collagen was constructed in the 10% PF-127/2% H-HPMC/0.05% NaOH embedding medium, crosslinked by NaOH and 37 °C, and then released to RT PBS. (G) A tetrahedron composed of 3.5% chitosan was printed in the 10% PF-127/3% H-HPMC/0.1% NaOH embedding medium, crosslinked by NaOH, and removed to RT PBS. (B-G) Subplots show the printed structures trapped in the embedding medium with various additives. (H) The embedding medium containing 10% PF-127, 2.5% H-HPMC, 0.1%  $\text{CaCl}_2$  and 1% GGT supported multi-material fabrication with different crosslinking methods. The alphabet 'Z' is composed of 5% GelMA which is photo-crosslinked. The alphabet 'J' is composed of 10% gelatin which is enzymatically crosslinked. Meanwhile, the alphabet 'U' is composed of 4% alginate which is ionically crosslinked. They were printed, crosslinked, and removed from the embedding medium

to 37 °C PBS with shape integrity. (I) A triple-layered hollow tube composed of 5% GelMA (outer layer), 10% Gelatin (median layer), and 4% alginate (inner layer) is printed and crosslinked in the 10% PF-127/2.5% H-HPMC/0.1% CaCl<sub>2</sub>/1% GGT medium. The subplot shows the bright-field image of the structure. (Scale bars: 5 mm)

medium. It was then released from the medium to RT PBS (figure 6E). The printed fingers kept their cantilever features after being immersed in the PBS, showing its shape fidelity. Furthermore, a bifurcated tube composed of 1% collagen (pH = 4.3) was printed in 0.05% NaOH/10% PF-127/2% H-HPMC (pH = 8.2) and then stored at 37 °C to allow fibrillation (figure 6F). The tube could keep great shape fidelity and could stand in the PBS with the help of buoyance. Finally, a tetrahedron structure was made using 3.5% chitosan solution in the 0.1% NaOH/10% PF-127/3% H-HPMC medium. The pH value of the medium was 11.3 and that of the bioink was 5.6, making the chitosan solution undergo basification. It was immersed into RT PBS and showed a well-defined structure (figure 6G).

We selected a combination of crosslinking strategies: photo-crosslinking, enzymatic crosslinking, and ionic crosslinking methods, to demonstrate potential applications of this proposed medium in challenging multi-material printing. The pH-crosslinking and the temperature-crosslinking methods were excluded because of their confliction with the enzymatic crosslinking method. We used 5% GelMA, 10% gelatin, and 4% alginate solutions to construct the letters “ZJU”. After printing, these letters were exposed to a blue light source for three minutes and then kept for six hours to fully crosslink. The crosslinked letters were released from the medium and immersed into 37 °C PBS (figure 6H, movie S6). A tri-layered tube was also fabricated by the same method, whose outer, median, and inner layers were composed of 5% GelMA, 10% gelatin, and 4% alginate solutions, respectively (figure 6I).

In these efforts, we were able to construct well-defined structures in the embedding medium containing different crosslinkers; and we demonstrated this medium can support five kinds of crosslinking methods. Especially, as a typical biocompatible material, collagen could be fabricated successfully in the proposed medium. After we utilized cell-laden collagen solution to fabricate tubes, cell-laden tubes were cultured for three days. During the culture duration, high cell viability (>80%) was observed, showing the great potential of the bath (supporting information, and figure S12). Besides, it is expected for a wider range of hydrophilic bioinks, such as fibrin, hyaluronic acid, and other materials immiscible with the medium can be used. The proposed HP embedding medium provides a platform to build advanced tissue engineering scaffolds for a wide range of organ systems.

### 3.5 Enhanced Adhesion Writing Method Based on the HP Embedding Medium

Bioprinting aims to fabricate biologically relevant structures using tissue-like materials, whose mechanical properties are preferred to match the target application.



However, the conventional layer-by-layer 3D printing process compromises the bonding strength between adjacent printed strands and layers, therefore, limiting the mechanical integrities of the printed structures [61]. Herein, a versatile enhanced adhesion writing method (EAW) based on the versatility and ideal rheological properties of the HP embedding medium was proposed, regardless of the crosslinking method (figure 7A). It utilized the thermoresponsive rheological properties of the embedding medium and the bioink between 22 °C and 33 °C (figure 7B). In short, the bioink was printed at an ideal temperature to keep good printability and sequentially heated to a higher temperature (33 °C) facilitating coalescence between adjacent layers to strengthen the structural connection. The increased temperature resulted in higher viscosity and yield stress of the embedding medium, keeping the bioink in a fixed cavity and preventing out-diffusion of the deposited bioink. The prints were then removed from the medium once crosslinked. It is noted that the upper temperature here was set as 33 °C, which could maximize the viscosity of the 10% PF-127/3% H-HPMC medium while decrease the viscosity of temperature-sensitive materials, such as gelatin and GelMA. Meanwhile, this temperature was proven to hardly affect cell viability [62]. The upper temperature was adjustable for the embedding medium with different concentrations.

As the proof-of-concept study, several tubular specimens were fabricated using temperature-sensitive materials (5% GelMA, 15% GelMA, and 10% gelatin) and temperature-insensitive material (4% alginate and 3.5% chitosan) [63]. They were deposited in mediums containing various crosslinkers. After printing, the fabricated tubes were kept in the medium. The whole container was then conveyed to a thermostat water bath (33 °C). After being heated for 10 minutes, the temperature of the system reached a steady-state condition (figure S13). As the control group, other specimens were printed under the same condition while kept at RT for 10 minutes. All tubular specimens were then crosslinked, removed from the embedding medium, washed, and tested successively. It is noted that the thermoresponsive property of the neutral 1% collagen was opposed to GelMA or gelatin. Its viscosity increases with the increase of temperature (figure S14), therefore it was not utilized here.

Although crosslinked by different methods, all EAW printed specimens showed better mechanical strengths compared with the control group. For 5% GelMA, 10% gelatin, and 15% GelMA, the maximum strains were significantly increased by 65.8%, 71.9%, and 34.7%, respectively (figure 7C-D). Meanwhile, the maximum strains increased by 12.8% for 4% alginate without significance. The crosslinked chitosan specimen by basification was too fragile to undergo the tensile test, its data were thus not available [63]. The differences in the enhanced maximum strain might attribute to the temperature sensitivity of each material. For the temperature-sensitive materials, the viscosity decreased dramatically as the temperature increased, facilitating the coalescence of adjacent layers. Thus, the bonding strength between adjacent layers was

enhanced markedly, even leading to a change of failure mode (figure 7C). While the temperature-insensitive material could only be enhanced to a small extent because of

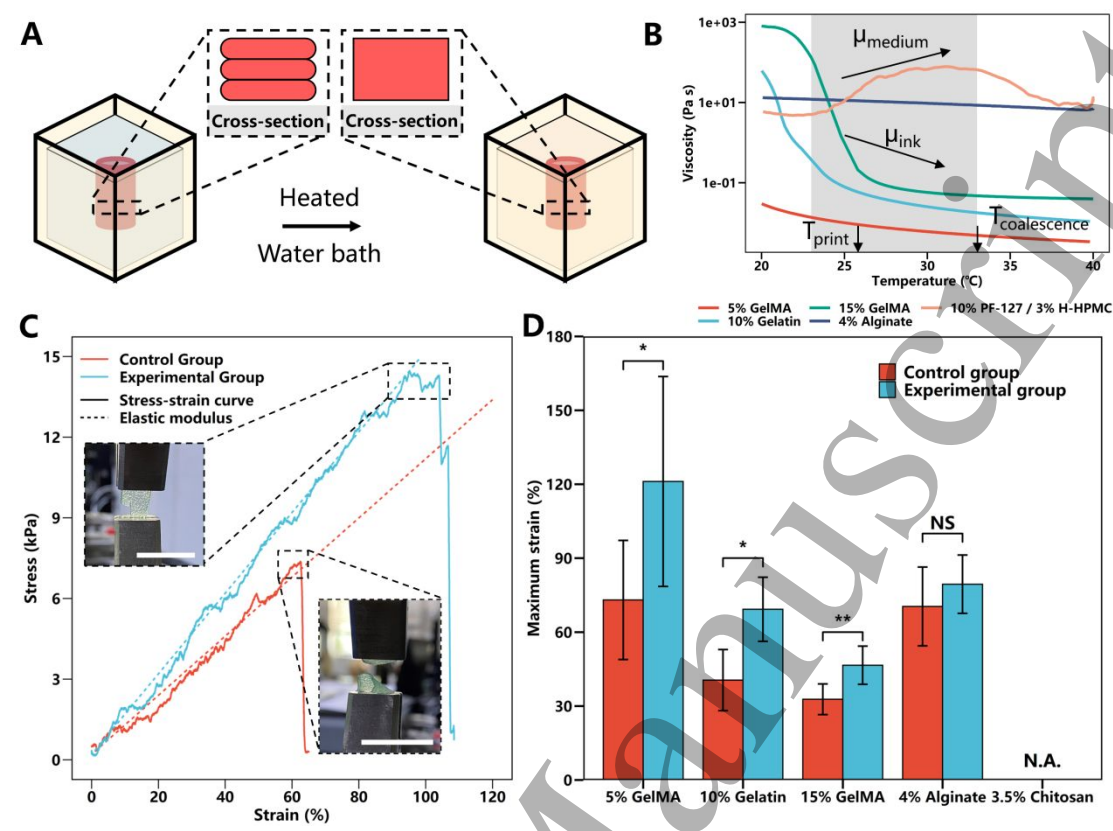


**Figure 7. Enhanced adhesion writing method based on the HP embedding medium.** (A) A schematic illustration of the enhanced adhesion writing method. Bioink is deposited in the HP embedding medium to form a tubular specimen, and then heated to strengthen the strand-by-strand adhesion by coalescence. (B) The thermoresponsive of the embedding medium and the bioink. (Black arrow: the operation temperature) (C) The representative stress-strain curves of the specimen consisting of 10% gelatin. The subplots show representative failure mode. (D) Maximum strain before the break of the specimens. (Scale bars: 25 mm. Data are plotted as mean  $\pm$  S.D., \* =  $p < 0.05$ ; \*\* =  $p < 0.01$ )

the tiny change of viscosity. Besides, the elastic modulus of the EAW printed specimens increased 23.9%, 36.6%, and 46.3%, respectively, for 5% GelMA, 10% gelatin, and 15% GelMA, without significance. This might attribute to the uncertainty in determining the exact cross-sectional area of the gage region.

In addition, the influence of the proposed method on the shape fidelity was evaluated, in which, bifurcated structures with featured angles were printed using 5% GelMA, 15% GelMA, 4% alginate, and 10% gelatin. The samples in the experimental group were post-processed at 33 °C for 10 min, and the samples in the control group were kept at RT for 10 min. After fully crosslinked, they were extracted and observed. As shown in figure S15, no statistical difference in the featured angle was detected

between the two groups, indicating that the proposed method could keep the shape fidelity and enhance the adhesion.

Based on the rheological properties of the HP embedding medium, the proposed EAW method can strengthen the bonding adhesion between adjacent strands significantly, regardless of the crosslinking methods. And it does not affect the shape fidelity. It might address the instinct adhesion issues between adjacent strands. While we have taken several materials as demonstrations, the advance presented here is extensible to printing other materials with similar rheological properties.

#### 4. Conclusion

In conclusion, a versatile embedding medium for multi-crosslinking printing was first developed via the controllable hydrophobic association between the H-HPMC and PF-127. The composition empowered the medium to have tunable rheological properties, good stability, and compatibility with additives without strong hydrophilic groups, which means the medium is compatible with the majority of bioink choices, facilitating multi-material printing. The HP embedding medium enabled freeform writing of the millimetric complex tubular structures, which could be released from the medium with high precision, shape fidelity, and perfused without leakage. High cell viability (more than 85%) and cell proliferation ability within the fabricated cell-laden tubular structures were observed within the culture duration. We successfully patterned three materials with different crosslinking methods in one medium, using the optimized compound and printing parameters, and we constructed strength-enhanced tubular structures using the versatile EAW method. Compared to the existing embedding mediums, the proposed HP embedding medium lays the groundwork for multi-material well-defined tissue-like structures fabrication due to its tunable printing window, good stability, biocompatibility, versatility to crosslinkers, and ease of removal. Though the bioinks used in the demonstration are limited, it is expected that a wide range of biological materials with different crosslinking methods, such as fibrin, and hyaluronic acid, can be printed in the medium. Thus, the medium could serve as a promising platform for multi-material bioprinting, facilitating the biofabrication of heterogeneous tissues/organs in vitro and opening unique prospects for personalized organ replacement and transplantation.

#### Acknowledgments

We would like to thank the support by National Key Research and Development Program of China (2018YFA0703000), National Natural Science Foundation of China (Grant No. 52105310, No. 51875518). Z.J. acknowledge the Jardine Foundation for financial support.

# References

- [1] Levato R, Jungst T, Scheuring R G, Blunk T, Groll J and Malda J 2020 From Shape to Function: The Next Step in Bioprinting *Adv. Mater.* **32** 1906423
- [2] Zhang Y S and Khademhosseini A 2020 Engineering in vitro human tissue models through bio-design and manufacturing *Bio-Des. Manuf.* **3** 155-9
- [3] Santoni S, Gugliandolo S G, Sponchioni M, Moscatelli D and Colosimo B M 2021 3D bioprinting: current status and trends—a guide to the literature and industrial practice *Bio-Des. Manuf.* **5** 14-42
- [4] Gillispie G, Prim P, Copus J, Fisher J, Mikos A G, Yoo J J, Atala A and Lee S J 2020 Assessment methodologies for extrusion-based bioink printability *Biofabrication* **12** 022003
- [5] Li Q, Zhang B, Xue Q, Zhao C, Luo Y, Zhou H, Ma L, Yang H and Bai D 2021 A Systematic Thermal Analysis for Accurately Predicting the Extrusion Printability of Alginate-Gelatin-Based Hydrogel Bioinks *Int. J. Bioprint.* **7** 394
- [6] Cooke M E and Rosenzweig D H 2021 The rheology of direct and suspended extrusion bioprinting *APL Bioeng.* **5** 011502
- [7] Lee A, Hudson A R, Shiowski D J, Tashman J W, Hinton T J, Yerneni S, Bliley J M, Campbell P G and Feinberg A W 2019 3D bioprinting of collagen to rebuild components of the human heart *Science* **365** 482-7
- [8] Bhattacharjee T, Zehnder S M, Rowe K G, Jain S, Nixon R M, Sawyer W G and Angelini T E 2015 Writing in the granular gel medium. *Sci. Adv.* **1** e1500655
- [9] Hinton T J, Jallerat Q, Palchesko R N, Park J H, Grodzicki M S, Shue H-J, Ramadan M H, Hudson A R and Feinberg A W 2015 Three-dimensional printing of complex biological structures by freeform reversible embedding of suspended hydrogels *Sci. Adv.* **1** e1500758
- [10] O'Bryan C S, Bhattacharjee T, Hart S, Kabb C P, Schulze K D, Chilakala I, Sumerlin B S, Sawyer W G and Angelini T E 2017 Self-assembled micro-organogels for 3D printing silicone structures *Sci. Adv.* **3** e1602800
- [11] Mirdamadi E, Tashman J W, Shiowski D J, Palchesko R N and Feinberg A W 2020 FRESH 3D Bioprinting a Full-Size Model of the Human Heart *ACS Biomater. Sci. Eng.* **6** 6453-9
- [12] Jeon O, Lee Y B, Jeong H, Lee S J, Wells D and Alsberg E 2019 Individual cell-only bioink and photocurable supporting medium for 3D printing and generation of engineered tissues with complex geometries *Mater. Horiz.* **6** 1625-31
- [13] Moxon S R, Cooke M E, Cox S C, Snow M, Jeys L, Jones S W, Smith A M and Grover L M 2017 Suspended Manufacture of Biological Structures *Adv. Mater.* **29**
- [14] Gong Y, Bi Z, Bian X, Ge A, He J, Li W, Shao H, Chen G and Zhang X 2020 Study on linear bio-structure print process based on alginate bio-ink in 3D bio-fabrication *Bio-Des. Manuf.*
- [15] Xie Z T, Kang D H and Matsusaki M 2021 Resolution of 3D bioprinting inside bulk gel and granular gel baths *Soft Matter* **17** 8769-85
- [16] Wu W, DeConinck A and Lewis J A 2011 Omnidirectional printing of 3D microvascular networks *Adv. Mater.* **23** H178-83
- [17] Colly A, Marquette C and Courtial E J 2021 Poloxamer/Poly(ethylene glycol) Self-Healing Hydrogel for High-Precision Freeform Reversible Embedding of Suspended Hydrogel *Langmuir* **37** 4154-62
- [18] Afghah F, Altunbek M, Dikyol C and Koc B 2020 Preparation and characterization of nanoclay-hydrogel composite support-bath for bioprinting of complex structures *Sci. Rep.* **10** 5257

- 1
  - 2
  - 3
  - 4
  - 5
  - 6
  - 7
  - 8
  - 9
  - 10
  - 11
  - 12
  - 13
  - 14
  - 15
  - 16
  - 17
  - 18
  - 19
  - 20
  - 21
  - 22
  - 23
  - 24
  - 25
  - 26
  - 27
  - 28
  - 29
  - 30
  - 31
  - 32
  - 33
  - 34
  - 35
  - 36
  - 37
  - 38
  - 39
  - 40
  - 41
  - 42
  - 43
  - 44
  - 45
  - 46
  - 47
  - 48
  - 49
  - 50
  - 51
  - 52
  - 53
  - 54
  - 55
  - 56
  - 57
  - 58
  - 59
  - 60
- [19] Kim J and Hyun J 2021 Soft Magnetostrictive Actuator String with Cellulose Nanofiber Skin *ACS Appl. Mater. Interfaces* **13** 43904-13
- [20] Shin S and Hyun J 2021 Rheological properties of cellulose nanofiber hydrogel for high-fidelity 3D printing *Carbohydr. Polym.* **263** 117976
- [21] Shin S, Kwak H, Shin D and Hyun J 2019 Solid matrix-assisted printing for three-dimensional structuring of a viscoelastic medium surface *Nat. Commun.* **10** 4650
- [22] Highley C B, Rodell C B and Burdick J A 2015 Direct 3D Printing of Shear-Thinning Hydrogels into Self-Healing Hydrogels *Adv. Mater.* **27** 5075-9
- [23] Song K H, Highley C B, Rouff A and Burdick J A 2018 Complex 3D-Printed Microchannels within Cell-Degradable Hydrogels *Adv. Funct. Mater.* **28**
- [24] Jin Y, Compaan A, Chai W and Huang Y 2017 Functional Nanoclay Suspension for Printing-Then-Solidification of Liquid Materials *ACS Appl. Mater. Interfaces* **9** 20057-66
- [25] Mahmoudi M, Burlison S R, Moreno S and Minary-Jolandan M 2021 Additive-Free and Support-Free 3D Printing of Thermosetting Polymers with Isotropic Mechanical Properties *ACS Appl. Mater. Interfaces* **13** 5529-38
- [26] Ning L, Mehta R, Cao C, Theus A, Tomov M, Zhu N, Weeks E R, Bauser-Heaton H and Serpooshan V 2020 Embedded 3D Bioprinting of Gelatin Methacryloyl-Based Constructs with Highly Tunable Structural Fidelity *ACS Appl. Mater. Interfaces* **12** 44563-77
- [27] Karyappa R and Hashimoto M 2021 Freeform Polymer Precipitation in Microparticulate Gels *ACS Appl. Polym. Mater.* **3** 908-19
- [28] Zhao J, Hussain M, Wang M, Li Z and He N 2020 Embedded 3D printing of multi-internal surfaces of hydrogels *Addit. Manuf.* **32**
- [29] Romanazzo S, Molley T G, Nemec S, Lin K, Sheikh R, Gooding J J, Wan B, Li Q, Kilian K A and Roohani I 2021 Synthetic Bone - Like Structures Through Omnidirectional Ceramic Bioprinting in Cell Suspensions *Adv. Funct. Mater.* **31**
- [30] Blaeser A, Duarte Campos D F, Puster U, Richtering W, Stevens M M and Fischer H 2016 Controlling Shear Stress in 3D Bioprinting is a Key Factor to Balance Printing Resolution and Stem Cell Integrity *Adv. Healthc. Mater.* **5** 326-33
- [31] Compaan A M, Song K and Huang Y 2019 Gellan Fluid Gel as a Versatile Support Bath Material for Fluid Extrusion Bioprinting *ACS Appl. Mater. Interfaces* **11** 5714-26
- [32] LeBlanc K J, Niemi S R, Bennett A I, Harris K L, Schulze K D, Sawyer W G, Taylor C and Angelini T E 2016 Stability of High Speed 3D Printing in Liquid-Like Solids *ACS Biomater. Sci. Eng.* **2** 1796-9
- [33] Grosskopf A K, Truby R L, Kim H, Perazzo A, Lewis J A and Stone H A 2018 Viscoplastic Matrix Materials for Embedded 3D Printing *ACS Appl. Mater. Interfaces* **10** 23353-61
- [34] Thielicke W and Sonntag R 2021 Particle Image Velocimetry for MATLAB: Accuracy and enhanced algorithms in PIVlab *J. Open Res. Softw.* **9**
- [35] Okubo M, Iohara D, Anraku M, Higashi T, Uekama K and Hirayama F 2020 A thermoresponsive hydrophobically modified hydroxypropylmethylcellulose/cyclodextrin injectable hydrogel for the sustained release of drugs *Int. J. Pharmaceut* **575** 118845

- [36] Iohara D, Okubo M, Anraku M, Uramatsu S, Shimamoto T, Uekama K and Hirayama F 2017 Hydrophobically Modified Polymer/ $\alpha$ -Cyclodextrin Thermoresponsive Hydrogels for Use in Ocular Drug Delivery *Mol. Pharmaceutics* **14** 2740-8
- [37] Malmsten M and Lindman B 1992 Self-assembly in aqueous block copolymer solutions *Macromolecules* **25** 5440-5
- [38] Guvendiren M, Lu H D and Burdick J A 2012 Shear-thinning hydrogels for biomedical applications *Soft Matter* **8** 260-72
- [39] Owusu-Nkwantabisah S, Gillmor J, Bennett G, Slater G, Szakasits M, Rajeswaran M and Antalek B 2018 Thermal stiffening of hydrophobic association hydrogels *Polymer* **145** 374-81
- [40] Zhang Y, Lane M E and Moore D J 2020 An Investigation of the Influence of PEG 400 and PEG-6-Caprylic/Capric Glycerides on Dermal Delivery of Niacinamide *Polymers-Basel* **12**
- [41] Liu G, Li Y, Yang L, Wei Y, Wang X, Wang Z and Tao L 2017 Cytotoxicity study of polyethylene glycol derivatives *RSC Adv.* **7** 18252-9
- [42] Gjorevski N, Sachs N, Manfrin A, Giger S, Bragina M E, Ordonez-Moran P, Clevers H and Lutolf M P 2016 Designer matrices for intestinal stem cell and organoid culture *Nature* **539** 560-4
- [43] Pandit N K and Kisaka J 1996 Loss of gelation ability of Pluronic® F127 in the presence of some salts *Int. J. Pharmaceut* **145** 129-36
- [44] Ye W, Zhu L, Xia S and Zhang X 2018 Dual pH-/temperature-responsive and fluorescent hydrogel for controlled drug delivery *J. Polym. Eng.* **38** 371-9
- [45] Lee E J and Hong G P 2020 Effects of microbial transglutaminase and alginate on the water-binding, textural and oil absorption properties of soy patties *Food Sci. Biotechnol.* **29** 777-82
- [46] Bakht S M, Gomez-Florit M, Lamers T, Reis R L, Domingues R M A and Gomes M E 2021 3D Bioprinting of Miniaturized Tissues Embedded in Self-Assembled Nanoparticle-Based Fibrillar Platforms *Adv. Funct. Mater.*
- [47] Muth J T, Vogt D M, Truby R L, Menguc Y, Kolesky D B, Wood R J and Lewis J A 2014 Embedded 3D printing of strain sensors within highly stretchable elastomers *Adv. Mater.* **26** 6307-12
- [48] Jin Y, Zhao D and Huang Y 2018 Study of extrudability and standoff distance effect during nanoclay-enabled direct printing *Bio-Des. Manuf.* **1** 123-34
- [49] Kolesky D B, Truby R L, Gladman A S, Busbee T A, Homan K A and Lewis J A 2014 3D bioprinting of vascularized, heterogeneous cell-laden tissue constructs *Adv. Mater.* **26** 3124-30
- [50] Shie M Y, Lee J J, Ho C C, Yen S Y, Ng H Y and Chen Y W 2020 Effects of Gelatin Methacrylate Bio-ink Concentration on Mechano-Physical Properties and Human Dermal Fibroblast Behavior *Polymers-Basel* **12**
- [51] Rizwan M, Chan S W, Comeau P A, Willett T L and Yim E K F 2020 Effect of sterilization treatment on mechanical properties, biodegradation, bioactivity and printability of GelMA hydrogels *Biomed Mater* **15** 065017
- [52] Jain R K, Au P, Tam J, Duda D G and Fukumura D 2005 Engineering vascularized tissue *Nat. Biotechnol.* **23** 821-3

- [53] Grossi S, Grimaldi A, Congiu T, Parnigoni A, Campanelli G and Campomenosi P 2021 Human Primary Dermal Fibroblasts Interacting with 3-Dimensional Matrices for Surgical Application Show Specific Growth and Gene Expression Programs *Int. J. Mol. Sci.* **22**
- [54] Nichol J W, Koshy S T, Bae H, Hwang C M, Yamanlar S and Khademhosseini A 2010 Cell-laden microengineered gelatin methacrylate hydrogels *Biomaterials* **31** 5536-44
- [55] Bilici C, Tatar A G, Senturk E, Dikyol C and Koc B 2022 Bisulfite-initiated crosslinking of gelatin methacryloyl hydrogels for embedded 3D bioprinting *Biofabrication* **14**
- [56] Camasao D B and Mantovani D 2021 The mechanical characterization of blood vessels and their substitutes in the continuous quest for physiological-relevant performances. A critical review *Mater. Today Bio* **10** 100106
- [57] Wang P, Sun Y, Shi X, Shen H, Ning H and Liu H 2021 3D printing of tissue engineering scaffolds: a focus on vascular regeneration *Bio-Des. Manuf.* 1-35
- [58] Rocca M, Fragasso A, Liu W, Heinrich M A and Zhang Y S 2018 Embedded Multimaterial Extrusion Bioprinting *SLAS Technol.* **23** 154-63
- [59] Min S J, Lee J S, Nah H, Kim S H, Moon H J, Reis R L, Kwon I K and Heo D N 2021 Development of photo-crosslinkable platelet lysate-based hydrogels for 3D printing and tissue engineering *Biofabrication* **13**
- [60] Dikyol C, Altunbek M and Koc B 2021 Embedded multimaterial bioprinting platform for biofabrication of biomimetic vascular structures *J. Mater. Res.*
- [61] Christensen K, Davis B, Jin Y and Huang Y 2018 Effects of printing-induced interfaces on localized strain within 3D printed hydrogel structures *Mater. Sci. Eng., C* **89** 65-74
- [62] Ouyang L, Yao R, Zhao Y and Sun W 2016 Effect of bioink properties on printability and cell viability for 3D bioplotting of embryonic stem cells *Biofabrication* **8** 035020
- [63] Suo H, Zhang D, Yin J, Qian J, Wu Z L and Fu J 2018 Interpenetrating polymer network hydrogels composed of chitosan and photocrosslinkable gelatin with enhanced mechanical properties for tissue engineering *Mater. Sci. Eng., C* **92** 612-20